The Alignment and Phasing System for the Thirty Meter Telescope

Gary Chanan[a], Mitchell Troy[b], Ian Crossfield[b], Jerry Nelson[c], Terry Mast[c]

[a] University of California, Irvine, CA 92697
[b] Jet Propulsion Laboratory, California Institute of Technology, Pasadena, CA 91109
[c] University of California, Santa Cruz, CA 95064

ABSTRACT

The Thirty Meter Telescope (TMT) is a collaborative project between the California Institute of Technology (CIT), the University of California (UC), the Association of Universities for Research in Astronomy (AURA), and the Association of Canadian Universities for Research in Astronomy (ACURA). The Alignment and Phasing System (APS) for the Thirty Meter Telescope will be a Shack-Hartmann type camera that will provide a variety of measurements for telescope alignment, including segment tip/tilt and piston, segment figure, secondary and tertiary figure, and overall primary/secondary/tertiary alignment. The APS will be modeled after the Phasing Camera System (PCS), which performed most, but not all, of these tasks for the Keck Telescopes. We describe the functions of the APS, including a novel supplemental approach to measuring and adjusting the segment figures, which treats the segment aberrations as global variables.

Keywords: telescopes, segmented mirrors, optical alignment, phasing

1. INTRODUCTION

The primary mirror of the Thirty Meter Telescope is an array of 738 nearly identical mirror segments,[1] each of which is actively controlled in its three out-of-plane degrees of freedom. The segment control consists of two functions: alignment and stabilization. This paper describes the alignment function, which is carried out by the Alignment and Phasing System (APS). The APS uses starlight to determine the desired values of the three degrees of freedom of each segment to an accuracy of several nanometers. The stabilization system, similar to the one in use at the Keck telescopes,[2] maintains these degrees of freedom in the face of gravity and temperature changes (and to some extent wind forces) and is described elsewhere in these proceedings.[3]

The APS also makes segment figure measurements; these measurements are used to adjust the segment figures by means of warping harnesses. In this paper we show how one can improve the overall smoothness of the TMT primary by treating segment aberrations as global variables.

2. BACKGROUND: THE KECK PHASING CAMERA SYSTEM

The Keck Phasing Camera System[4] (PCS) uses starlight to perform four basic alignment functions for each of the Keck telescopes: tip/tilt of segments, piston of segments (phasing), co-alignment of primary and secondary mirrors, and figure measurements of individual segments. The cameras are used for several hours approximately once a month for the first three functions. The segment figure measurements are typically made only after segments have been exchanged for aluminization, as the segments must be adjusted whenever they are removed and re-installed in the telescope. The accuracies associated with each function are listed in Table 1.

The segment tip/tilts, segment figures, and primary/secondary co-alignment are all measured using traditional Shack-Hartmann tests, with the relevant subapertures lying entirely within the boundaries of individual segments; segment pistons are measured using a wave optics generalization of the Shack-Hartmann approach, with the subapertures straddling the edges between neighboring segments.[5]

The PCS cameras are permanently mounted at a bent Cassegrain focus on each of the Keck telescopes. Each camera has a 750 mm focal length collimating lens, which images the primary mirror onto an array of lenslets (or prisms in the case of the phasing function) at a magnification of 1/200. A beamsplitter permits the injection of a reference beam (a fiber optic coupled LED) into the camera in order to calibrate the downstream

Ground-based and Airborne Telescopes, edited by Larry M. Stepp, Proc. of SPIE
Vol. 6267, 62672V, (2006) · 0277-786X/06/$15 · doi: 10.1117/12.670894

optics, and a transmissive flat in the collimated beam allows fine registration of the re-imaged primary with respect to the lenslet array. Stellar subimages from the Shack-Hartmann subapertures are imaged onto a 1024 x 1024 Cassini CCD with 12 micron pixels. The image scale at the detector is 6.9 pixels per arcsecond and the separation between nearest neighbor phasing subimages, located at the midpoints of the intersegment edges, is 9.5 arcseconds. The cameras are approximately 1.5 meters long and 0.6 meters in diameter.

PCS determines the piston, tip, and tilt of the secondary mirror relative to the primary by measuring the effect of these misalignments on the apparent focus and astigmatism of the primary mirror segments. PCS makes on-axis measurements only. As a result, some misalignments, such as secondary tip/tilt and decenter, are degenerate. At Keck, this degeneracy is broken by simply ascribing all of the astigmatic error to secondary tip and tilt. TMT will utilize a more sophisticated approach to break this and related degeneracies.

Table 1. Keck PCS Alignment Accuracies †

Function	RMS accuracy
Segment Tip/Tilt	10 milli-arcsec (1-dim)
Segment Piston‡	6 nm
Segment 2nd Order	4 nm
Segment 3rd Order	2 nm
Secondary Piston	15 microns
Secondary Tip/Tilt	4 arcsec (1-dim)

† All numbers refer to surface, not wavefront, errors.
‡ The piston error is less than the corresponding intersegment edge height uncertainty because the segment pistons are overdetermined by the edge measurements.

3. OPTICAL DESIGN OF THE APS

The optical design of the APS is similar to that of PCS except that the magnification of the pupil is 1/600. The focal length of the collimator is again 750 mm. The tentative choice for the detector is a Fairchild CCD 486 with 4096 x 4096 15 micron pixels (61.4 mm image area). With lenslet focal lengths of 22 mm, the local image scale on the detector is 4 pixels per arcsecond. Figure 1 shows the nominal mapping of lenslets to a primary mirror segment. The hexagonal lenslets, which may be stopped down to circles, have an inscribed diameter of 15 cm mapped to the primary mirror, so that there are three lenslets per intersegment edge (not counting the vertex lenslets), and 37 interior lenslets. [The segment edges are 60 cm long.] For the remainder of this work, we shall mainly be concerned with the information contained in the images formed by the 18 edge-straddling subimages, but in a complete treatment of the problem, one would also utilize the information from the 37 interior lenslets. For this geometry there are 4 arcseconds between subimages. Both the image scale and the distance between nearest neighbor subimages are less favorable than the corresponding PCS parameters (6.9 pixels per arcsecond and 9.5 arcseconds between subimages respectively); detailed simulations will be carried out to see whether this is workable or whether a larger format CCD will ultimately be required to relieve subimage crowding.

Because of the additional adjustable degrees of freedom of the TMT secondary and tertiary mirrors compared to Keck, as well as the tighter TMT optical tolerances, the APS camera will have to make off-axis measurements, whereas the PCS cameras on Keck made only on-axis measurements. We currently plan to access a variety of field angles by deliberately misaligning the telescope tertiary. Motion of an additional mirror within APS will be required in order to realign the re-imaged primary mirror with the Shack-Hartmann optics within APS.

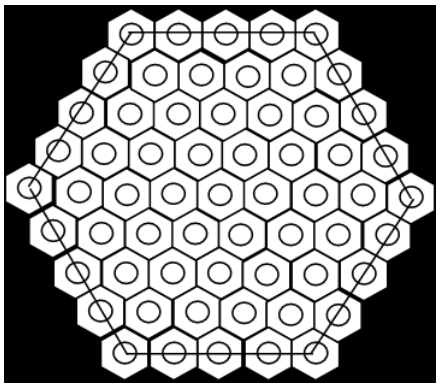

Figure 1. The proposed mapping of APS lenslets onto a TMT primary mirror segment. The lenslets are hexagonal, but may be stopped down to circular apertures.

4. EDGE SENSING AND SMOOTHING

At Keck, the division between wave optics measurements of the intersegment edge heights and Shack-Hartmann measurements for all other degrees of freedom is in some sense artificial, since the edge measurements contain information on the segment tip/tilts and figures (though the converse is not true: the former contain no information on segment pistons). In the following we investigate how the additional information can be extracted from the edge measurements and we provide a quantitative comparison of the two techniques.

Although the above two techniques may sound similar, there is a fundamental difference between them. In the traditional Shack-Hartmann test, the measurements on segments are local (pertaining only to the segment of interest), while the wave optics measurements of necessity treat edges as global variables, since more than one segment is involved in each measurement. This makes the edge measurements more difficult to deal with, as the problem is defined by a (very) large global control matrix, but there is also the potential benefit that one expects a globally smoother configuration of the primary mirror to result. This may be particulary important in the context of high contrast imaging. To emphasize this potential benefit we shall refer to the wave optics technique in the present context as "edge sensing and smoothing" or ESS.

In fact, in addition to global wavefront smoothness, there are other potential advantages to the edge based approach. Edge sensing and smoothing is based on measuring wavefront discontinuities, while Shack-Hartmann measurements are based on measuring wavefront slope errors. Since, apart from segmented mirrors, very few optical elements can introduce wavefront discontinuities, it is easier to limit systematic errors in the edge smoothing case. Careful measurements have established that the systematic errors associated with the phasing procedures used at Keck are less than 2 nm rms. At this level in the context of the Keck error budget these effects are not even worth bothering about, but it is conceivable that a correction could be applied to reduce them even below this small value. A related advantage is associated with the statistical contributions to the uncertainties that come from atmospheric turbulence in both measurement techniques. At Keck, a representative number for the uncertainty in each second order Zernike coefficient in a 600 second measurement on a 1.8 meter segment due to atmospheric turbulence is 3.9 nm; the corresponding overall segment surface uncertainty is 26 nm. Noethe[6] gives a corresponding estimate for the VLT 8-meter mirrors and 30 second integrations, which is consistent with this, assuming scaling with diameter and time of $d^{\,5/6}$ and $t^{-1/2}$. Scaling to the 1.2 meter TMT segments yields an overall segment surface uncertainty of 19 nm in 600 seconds. By comparison, once the n-lambda ambiguities are sorted out, we can measure piston errors to about 10 nm rms surface in only 30 seconds. [The dramatic difference is again due principally to the fact that atmospheric phase errors are quite continuous.] Thus edge sensing and smoothing offers the possibility of making measurements that are at least as accurace as, but twenty times faster than, the traditional Shack-Hartmann approach.* These potential advantages make ESS worth investigating,

*Although we speak of the atmospheric uncertainty as being associated with the Shack-Hartmann approach, it applies to any long-exposure, through-the-atmosphere wavefront sensing technique, for example, curvature sensing.

even if (as is shown below) there are also some significant potential shortcomings of this approach.

We assume that the Keck edge height measurement accuracy of 10 nm (rms) also obtains for the proposed geometry under consideration here. The TMT has 738 segments with a total of 2106 intersegment edges, so that three measurements per edge implies a total of 6318 edge height measurements. Suppose each segment is characterized by Zernike polynomials from piston, tip, and tilt, through 4th order. This is a total of 15 coefficients per segment, or 11070 for the entire primary mirror. The segment surface information is used to set warping harnesses which adjust the segment surface shapes. The warping harnesses have only limited degrees of freedom and the resulting surface adjustments will necessarily be incomplete. We expect that at most 10 degrees of freedom will be adjusted, but for the purposes of this initial study, we limit it to six: piston, tip, and tilt (controlled by the rigid body actuators of the active control system), and the three quadratics (two astigmatisms and one focus, controlled by the warping harnesses themselves). There are a total of 4428 of these segment degrees of freedom - fewer than the number of edge measurements - so that at least in principle one can hope to obtain a complete solution.

It is straightforward to construct the control matrix for the edge smoothing problem by a technique similar to that used to construct the corresponding matrix for the active control system of the telescope;[7] we do not reproduce the details here. If $\mathbf{z}$ is the vector of segment Zernike coefficients for all segments (with nominally 4428 components) and $\mathbf{e}$ is the vector of edge measurements for all apertures on all edges (with nominally 6318 components), then these two vectors are related by the control matrix $\mathbf{A}$:

$$\mathbf{e} = \mathbf{A}\,\mathbf{z}$$

and the desired best-fit Zernike vector $\mathbf{z_0}$ can be obtained using the pseudo-inverse $\mathbf{B}$ of the $\mathbf{A}$-matrix:

$$\mathbf{z_0} = \mathbf{B}\,\mathbf{e}$$

The preferred technique for constructing the pseudo-inverse $\mathbf{B}$ in the context of the present problem is singular value decomposition (SVD). This is particularly important as, depending upon the precise geometry, there may be a significant number of singular modes of the $\mathbf{A}$-matrix; that is, configurations of the primary mirror which cannot be sensed by the edge measurements. In general these singular modes are non-intuitive. The advantage of SVD over other matrix inversion schemes is that it automatically diagnoses and identifies these singular modes.

For the remainder of the present work, we will consider not the full 738 segment TMT, but rather a 126 segment telescope, with the segments arranged in 6 rings (and the central segment omitted). This has the advantage over the TMT that the computation time (limited by the singular value decomposition) is several hundred times faster, and also that the graphical representation of the segmentation of the pupil is clearer for the smaller number of segments. We assert that the behavior of the solution is at most weakly dependent on the number of segments, so that the results will be very similar for the TMT. We will examine this latter issue more carefully in a subsequent study.

Suppose we control 6 Zernike terms for each segment. Then the control matrix is 1008 (3 measurements on each of 336 intersegment edges) by 756 (6 Zernike polynomials on each of 126 segments). There are 44 singular modes for this geometry; four of these correspond to global piston, tip, tilt, and radius of curvature of the primary mirror, but most are non-intuitive. Figure 2 shows a few selected singular modes.

4.1. Case Studies

In this section we present several case studies of ESS simulations. Case 1 is an idealized, noise-free case which illustrates the method. Cases 2 and 3 demonstrate a problem with the method: due to a high level of noise propagation, it is virtually unstable, with the wavefront error growing rapidly even as the edge discontinuities are reduced. In Case 4 we present a way around this problem which involves suppressing a reasonably large number of modes in the control matrix.

Case 1: We first consider a 126-segment telescope with aberrations of 10 nm in each of the first 6 Zernike terms, and no higher aberrations. [We use the ordering and normalization of the Zernike polynomials of Noll.[8]] The rms values of the Zernike coefficients (averaged over segments) before and after the edge smoothing procedure are

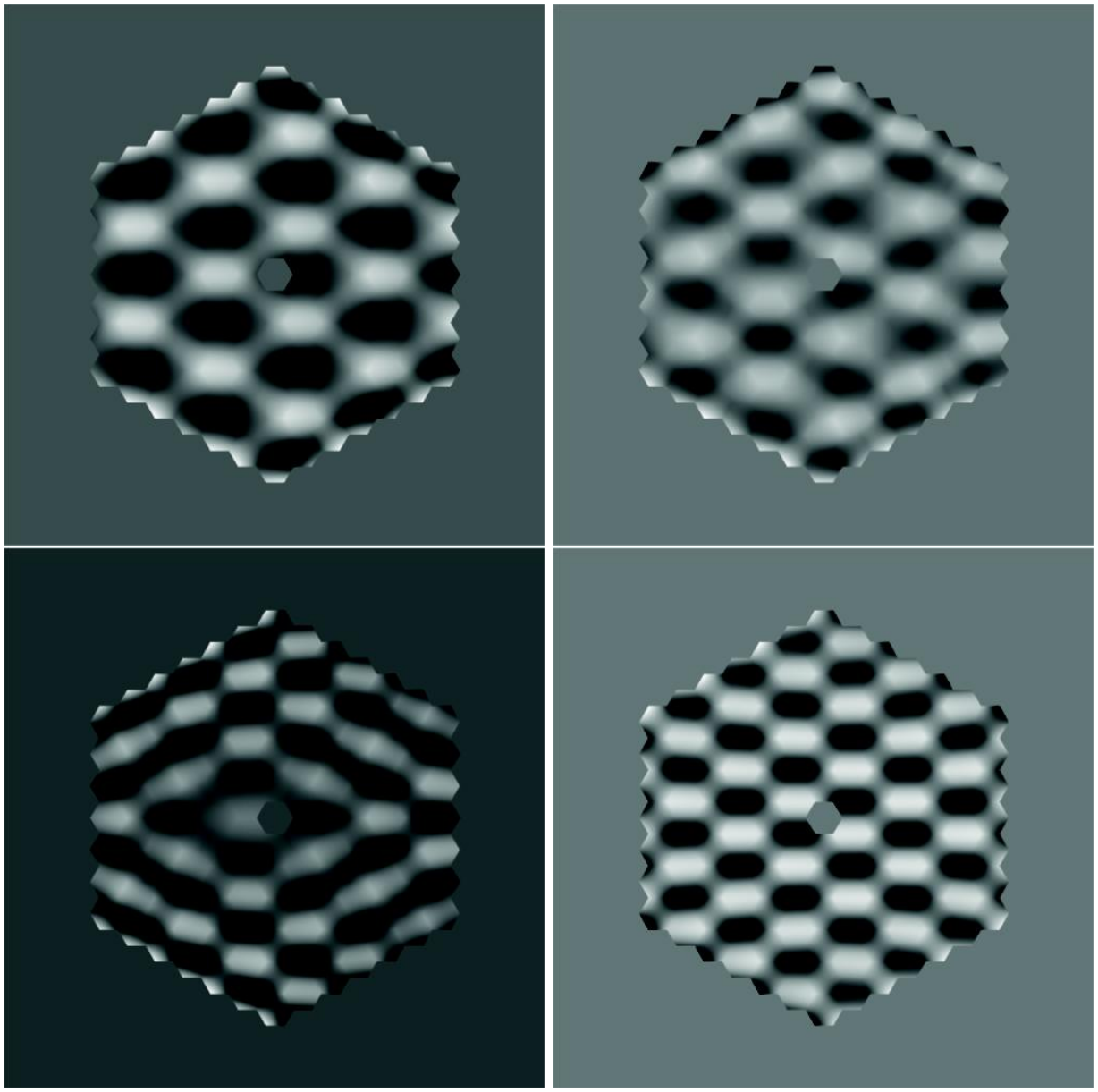

Figure 2. Four of the 44 singular modes for the edge sensing and smoothing problem for a six-ring segmented telescope (126 segments) with six degrees of freedom per segment. Familiar singular modes (not shown) are global piston, global tip and tilt, and global radius of curvature. However, most of the remaining singular modes, like the above, have no simple intuitive interpretation.

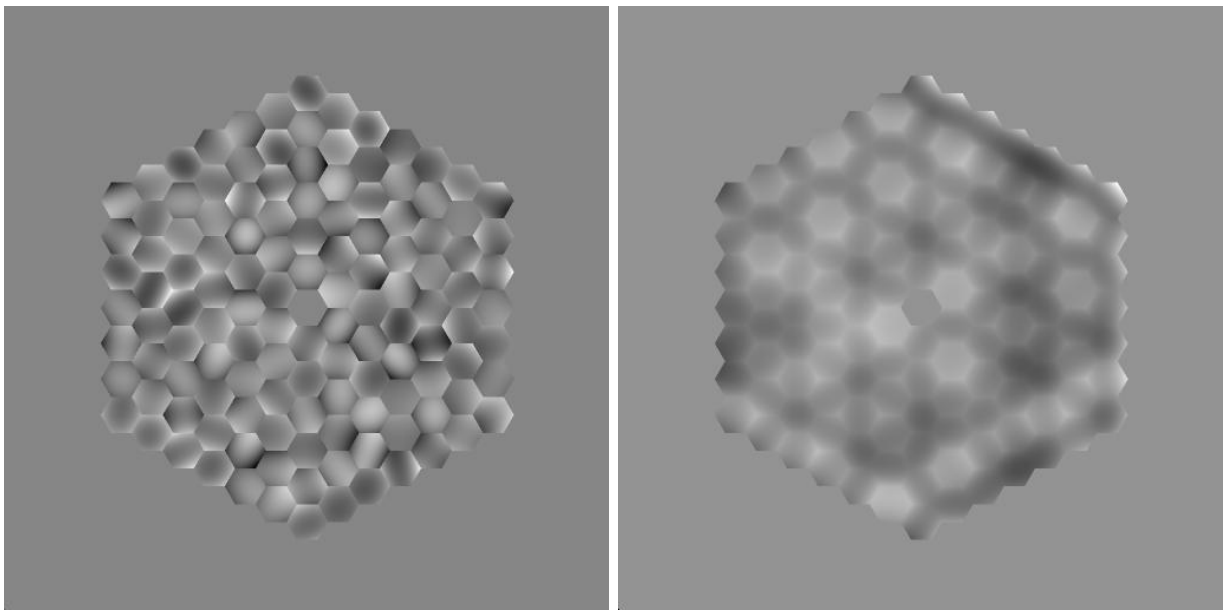

Figure 3. Phase map of a 126-segment mirror before (left) and after (right) the edge sensing and smoothing procedure for the idealized Case 1, in which all segment aberrations are represented in the control matrix. See Table 2 for a quantitative description of the wavefront errors before and after. The mapping from wavefront error to greyscale is the same in both panels.

shown in Table 2. The coefficients are reduced by factors of between 2 and 7, with the reduction factor increasing with the order of the term. There is no measurement noise in this simulation. The coefficients in the "After" column are not zero because they include contributions from the singular modes, which cannot be corrected. Both the qualitative improvement in the edge smoothness and the residual effects of the singular modes are obvious in Figure 3. However, even though the wavefront error is not zero, the rms edge height (averaged over the 1008 sites where the measurements take place) *is* reduced to zero from its original value of 40 nm. This is because the residual singular modes by definition have no contribution to the edge height. A useful check on the overall analysis is to remove the singular modes from the input ("Before") data; one can readily confirm that the "After" coefficients go to zero under these circumstances.

Case 2: This simulation is identical to Case 1 (including identical initial wavefront error), except this time we assume realistic errors in measuring the edge heights of 10 nm rms surface (not wavefront). The problem with the method is now evident in Table 2; although the edge discontinuities have again been reduced, this time from 40 to 8 nm, the final wavefront errors have grown by a factor of 20 to 40 relative to the noise free case, and in fact are as much as an order of magnitude larger even than the starting point wavefront errors. The problem is one of noise propagation in the control matrix. [The corresponding graphical representations of the pupil for this case, and for the similarly unstable Case 3 (below) are not shown.]

Case 3: This simulation is identical to Case 1, except this time we assume wavefront errors in higher order than those considered by the control matrix. To be specific, the control matrix again includes terms only through second order (6 terms) but we now include 10 nm aberrations in all terms through third order (10 terms). For the moment we again assume zero measurement errors. The results are shown in Table 2. As in Case 2, the edge discontinuities have been reduced, from 49 nm to 5 nm, but the wavefront errors have grown even more than in Case 2. The problem is evidently that the higher order terms act as an effective noise source; in fact, since they are systematic and not random, their effect is even more devastating than in Case 2. [From this perspective it makes little difference if one does or does not include measurement noise together with the higher order terms.] This case is significant because it is inevitable that there will be higher order contributions than we can successfully model, thus this instability is a serious concern.

Table 2. Results of Edge Sensing and Smoothing for Various Cases

Zernike†	Analysis‡	RMS Before	RMS After	RMS After
		(microns)	Case 1 (microns)	Case 2 (microns)
1	1	0.0102	0.0046	0.1741
2	1	0.0094	0.0018	0.0480
3	1	0.0098	0.0019	0.0597
4	1	0.0106	0.0015	0.0352
5	1	0.0091	0.0017	0.0236
6	1	0.0094	0.0012	0.0255
edge	—	0.0398	0.0000	0.0081
			Case 3	Case 4
1	1	0.0102	0.8285	0.0100
2	1	0.0094	0.1673	0.0172
3	1	0.0098	0.2660	0.0180
4	1	0.0106	0.0354	0.0104
5	1	0.0091	0.0720	0.0156
6	1	0.0094	0.0558	0.0165
7	0	0.0087	0.0087	0.0087
8	0	0.0100	0.0100	0.0100
9	0	0.0096	0.0096	0.0096
10	0	0.0095	0.0095	0.0095
edge	—	0.0489	0.0046	0.0119
			Case 5	Case 6
1	1	0.0102	0.1675	0.0183
2	1	0.0094	0.0410	0.0168
3	1	0.0098	0.0378	0.0204
4	1	0.0106	0.0106	0.0106
5	1	0.0091	0.0091	0.0091
6	1	0.0094	0.0094	0.0094
edge	—	0.0398	0.0096	0.0137

† Zernike index and normalization as in Noll.[8]

‡ A "1" in the Analysis column means that the corresponding aberration is represented in the control matrix; a "0" means that it is not.

4.2. Stabilizing the ESS Algorithm

In this section we explore a technique for stabilizing the edge smoothing algorithm. In some sense the difficulty with edge smoothing as defined above is that it tries to minimize the rms edge step and in general it does so successfully, but with no penalty for increasing the overall wavefront error. One can imagine a variety of ways to limit the wavefront error (in general accepting a small increase in the rms edge step). A simple method can be readily implemented into the SVD analysis utilized above.

In the context of the present problem, SVD describes the possible configurations of the primary mirror as linear combinations of 756 linearly independent modes. Traditionally, one excludes those modes (44 in the present problem) which are singular in the sense that the diagonal elements w_j of the **W**-matrix in the usual SVD notation[9] (generally called the "singular values" whether or not the corresponding modes are truly singular) are identically zero or are within numerical errors of zero. We eliminate singular modes from the solution because including them could increase the wavefront errors while doing nothing whatsoever to reduce the size of the edge discontinuity. Here we propose to eliminate as well many additional modes with merely small values of w_j on the grounds that this should constrain the growth of the wavefront error and only have a modest effect on our ability to minimize the edge discontinuity. A typical trial is shown as Case 4 below.

Case 4: This simulation is identical to Case 3, except that this time the 300 modes with the smallest w_j have been eliminated from the solution. [This is readily done within the context of the SVD algorithm, which normally allows one to specify a threshold on w_j.] These 300 modes include the 44 ordinary singular modes and an additional 256 suppressed modes with small but non-zero values of w_j. As in Case 3, aberrations in higher order modes have been included, and since this tends to be dominant, we have not included the effects of measurement noise. As expected, the reduction of the edge rms is not as dramatic as before: it is reduced from 49 to 12 nm, compared to the former 5 nm. However, the unstable growth of the wavefront error has been dramatically curtailed; instead of a factor of 80 increase, the wavefront error has grown by less than a factor of 2. [See Figure 4 for representations of the before and after pupils for this case.] As in Case 3, including realistic measurement errors does not significantly change these results, because the effective noise due to the higher order terms dominates over actual measurement noise.

The fact that the wavefront error has increased and not decreased is not a fatal problem, but it does require some comment. It is probable that the edge sensing and smoothing algorithm would be used as a last step in the alignment process. In the first steps, the segment aberrations would be measured (and then reduced) using Shack-Hartmann measurements in the interior subapertures in the lenslet array (see Figure 1). This is necessary not only to limit the ESS singular and suppressed modes, but because the wave optics procedure on which ESS is based requires that the edge heights not exceed about 100 nm rms in order to avoid aliasing problems.[10] In the last stages, growth of the wavefront error is tolerable because it will be only modest (since the algorithm is linear) and since the resulting tradeoff of wavefront error for edge smoothness is probably worthwhile, since adaptive optics systems are better able to correct smoother wavefronts.

4.3. ESS for Segment Piston and Tip/Tilt Adjustment

Note that considerations similar to the above apply even if the segment shapes are not adjustable. Suppose that we can only adjust the segments in their rigid body degrees of freedom of piston, tip, and tilt. Edge measurements are always required to determine segment pistons, but we can use either Shack-Harmann measurements or ESS to determine segment tip/tilts. The latter case is quite analogous to those discussed above, except that there are fewer degrees of freedom. In Cases 5 and 6 below, we use ESS to measure and adjust segment tip/tilts. In both cases we assume that the measurement uncertainties are principally due to segment aberrations, in these cases 10 nm of each of the three second order terms (two astigmatisms plus focus); measurement errors are not included. The only true singular modes for this geometry are the familiar four global modes: piston, tip, tilt, and radius of curvature.

In Case 5 (see Table 2) we apply ESS with only the four true singular modes excluded. The edge discontinuity is decreased from 40 to 10 nm, but the piston and tip/tilt errors are increased from the original 10 nm to 167 and 40 nm respectively. In Case 6 (see Figure X) we apply ESS but with an additional 57 modes suppressed; this time the final piston and tip/tilt errors are all within the range 17 to 20 nm, and the edge discontinuity is still

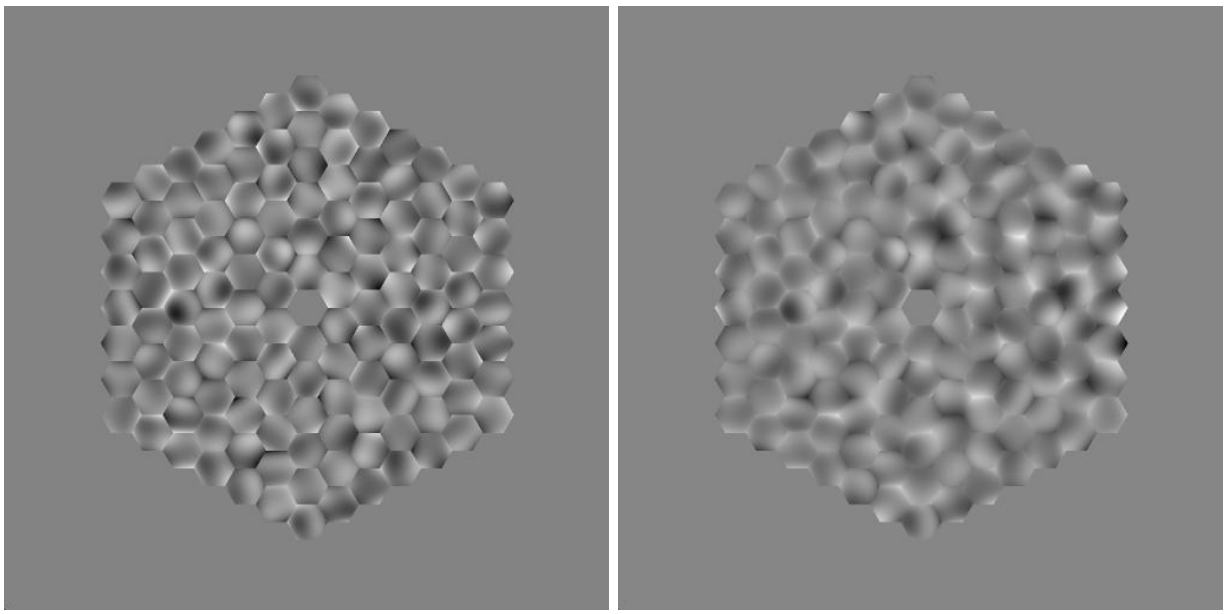

Figure 4. Phase map of a 126-segment mirror before (left) and after (right) the edge sensing and smoothing procedure for Case 4 - not all segment aberrations are represented in the control matrix, and 256 mirror modes are suppressed. See Table 2 for a quantitative description of the wavefront errors before and after. The mapping from wavefront error to greyscale is the same in both panels.

reduced, although now only to 14 nm (but this is still nearly three times smaller than the original unsmoothed value). See Figure 6 for before and after representations of the pupil for Case 6. [Case 5 is not shown.]

5. SUMMARY

The APS camera will perform alignment and phasing functions for the TMT similar to the way in which the PCS cameras successfully perform these functions for the Keck telescopes. However, the APS may utilize a wave-optics-based edge measuring technique which we call ESS, to supplement the traditional geometrical-optics-based Shack-Hartmann technique. ESS produces mirror configurations which are more continuous than techniques that treat segments locally. The ESS technique is potentially unstable in that the wavefront errors can grow rapidly as the intersegment edge discontinuities are reduced, but we have shown how the technique can be stabilized by suppressing a number of mirror modes in the control algorithm.

ACKNOWLEDGMENTS

This research was carried out in part at the Jet Propulsion Laboratory, California Institute of Technology, and was partially supported by the California Institute of Technology and the National Aeronautics and Space Administration.

The authors gratefully acknowledge the support of the TMT partner institutions. They are the Association of Canadian Universities for Research in Astronomy (ACURA), the Association of Universities for Research in Astronomy (AURA), the California Institute of Technology and the University of California. This work was supported, as well, by the Canada Foundation for Innovation, the Gordon and Betty Moore Foundation, the National Optical Astronomy Observatory, which is operated by AURA under cooperative agreement with the National Science Foundation, the Ontario Ministry of Research and Innovation, and the National Research Council of Canada.

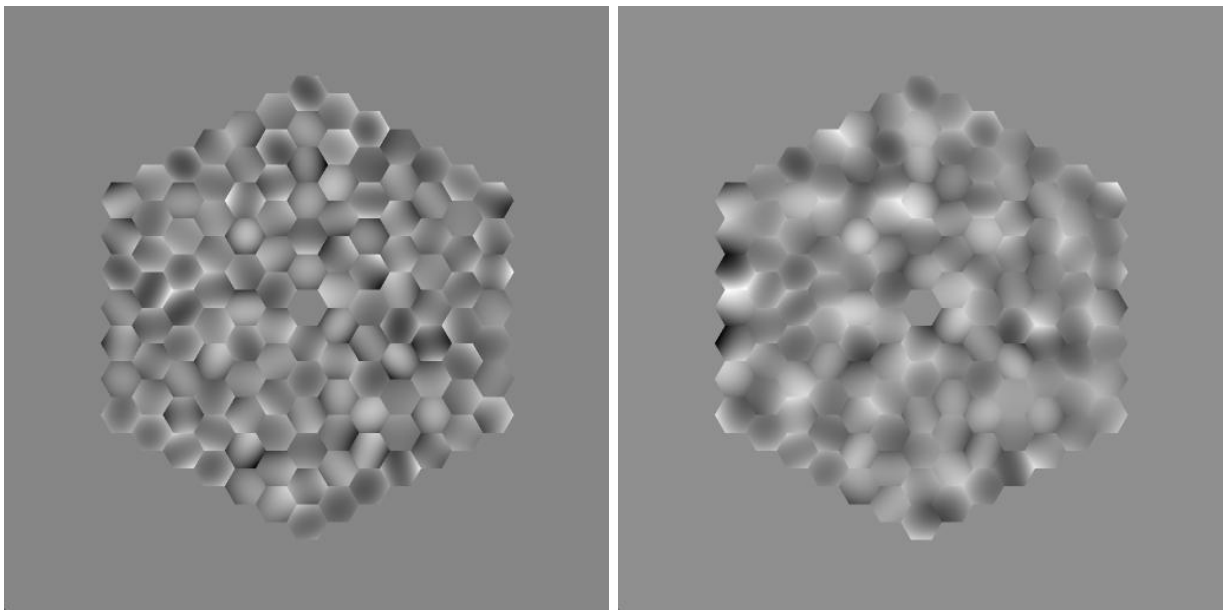

Figure 5. Phase map of a 126-segment mirror before (left) and after (right) the edge sensing and smoothing procedure for the parameters in Case 6 - segment aberrations are not represented in the control matrix, which only includes piston, tip, and tilt, and 57 mirror modes are suppressed. For a quantitative characterization of the mirror (before and after) see Table 2. The mapping from wavefront error to greyscale is the same in both panels.

REFERENCES

1. J. E. Nelson and G. H. Sanders, "TMT Status Report," in *Ground-based and Airborne Telescopes*, L. M. Stepp, ed., SPIE **6267** [this volume], 2006.
2. R. Cohen, T. Mast, and J. Nelson, "Performance of the W. M. Keck Telescope active mirror control system," in *Advanced Technology Optical Telescopes V*, L. M. Stepp, ed., SPIE **2199**, pp. 105-116, 1994.
3. T. S. Mast, G. A. Chanan, J. E. Nelson, R. H. Minor, and R. C. Jared, "An Edge Sensor Design for the Thirty Meter Telescope," in *Ground-based and Airborne Telescopes*, L. M. Stepp, ed., SPIE **6267** [this volume], 2006.
4. G. A. Chanan, "Design of the Keck Observatory alignment camera," in *Precision Instrument Design*, T. C. Bristow and A. E. Hathaway, eds., SPIE **1036**, pp. 59-70, 1988.
5. G. A. Chanan, M. Troy, F. G. Dekens, S. Michaels, J. Nelson, T. Mast, and D. Kirkman, "Phasing the mirror segments of the Keck telescopes: the broadband phasing algorithm," Applied Optics **37**, pp. 140-155, Jan. 1998.
6. L. Noethe,"Active Optics in Modern, Large Optical Telescopes," Progress in Optics **43**, (2002)
7. G. Chanan, D. G. MacMartin, J. Nelson, and T. Mast, "Control and Alignment of Segmented-Mirror Telescopes: Matrices, Modes and Error Propagation," Applied Optics **43**, pp. 1223-1232, 2004.
8. R. J. Noll, "Zernike polynomials and atmospheric turbulence," J. Opt. Soc. Am. **66**, 207 (1976).
9. W. H. Press, B. P. Flannery, S. A. Teukolsky, and W. T. Vetterling, "Numerical Recipes: The Art of Scientific Computing," Cambridge University Press, 1986.
10. G. A. Chanan, C. Ohara, M. Troy, "Phasing the mirror segments of the Keck telescopes: the narrowband phasing algorithm," Applied Optics **39**, pp. 4706-4714, Sept. 2000.